Transcriptional downregulation of FAM3C/ILEI in the Alzheimer's brain

Naoki Watanabe[1], Masaki Nakano[1], Yachiyo Mitsuishi[1], Norikazu Hara[2], Tatsuo Mano[3], Atsushi Iwata[3, 4], Shigeo Murayama[4], Toshiharu Suzuki[5], Takeshi Ikeuchi[2], Masaki Nishimura[1,*]

[1] Molecular Neuroscience Research Center, Shiga University of Medical Science, Shiga 520-2192, Japan,

[2] Department of Molecular Genetics, Brain Research Institute, Niigata University, Niigata 951-8585, Japan.

[3] Department of Neurology, Graduate School of Medicine, The University of Tokyo, Tokyo 113-8655, Japan,

[4] Department of Neuropathology, Tokyo Metropolitan Institute of Gerontology, Tokyo 173-0015, Japan,

[5] Laboratory of Neuroscience, Graduate School of Pharmaceutical Sciences, Hokkaido University, Hokkaido 060-0812, Japan,

*To whom correspondence should be addressed to Masaki Nishimura, Tel: +81-77-548-2328, Fax: +81-77-548-2210; E-mail: mnishimu@belle.shiga-med.ac.jp.

Abstract

Amyloid-β (Aβ) accumulation in the brain triggers the pathogenic cascade for Alzheimer's disease (AD) development. The secretory protein FAM3C (also named ILEI) is a candidate for an endogenous suppressor of Aβ production. In this study, we found that FAM3C expression was transcriptionally downregulated in the AD brain. To determine the transcriptional mechanism of the human *FAM3C* gene, we delineated the minimal 5′-flanking sequence required for basal promoter activity. From a database search for DNA-binding motifs, expression analysis using cultured cells, and promoter DNA-binding assays, we identified SP1 and EBF1 as candidate basal transcription factors for *FAM3C*, and found that SMAD1 was a putative inducible transcription factor and KLF6 was a transcription repressor for *FAM3C*. Genomic deletion of the basal promoter sequence from HEK293 and Neuro-2a cells markedly reduced endogenous expression of FAM3C and abrogated SP1- or EBF1-mediated induction of FAM3C. Nuclear protein extracts from AD brains contained lower levels of SP1 and EBF1 than did those from control brains, although the relative mRNA levels of these factors did not differ significantly between the groups. Additionally, the ability of nuclear SP1 and EBF1 in AD brains to bind with the basal promoter sequence-containing DNA probe was reduced compared with the binding ability of these factors in control brains. Thus, the transcriptional downregulation of FAM3C in the AD brain is attributable to the reduced nuclear levels and genomic DNA binding of SP1 and EBF1. An expressional decline in FAM3C may be a risk factor for Aβ accumulation and eventually AD development.

Introduction

Alzheimer's disease (AD) is the major cause of elderly dementia; it is characterized by two neuropathological signatures: amyloid plaques and neurofibrillary tangles, which represent insoluble depositions of amyloid-β (Aβ) peptides and hyperphosphorylated tau proteins, respectively (1, 2). Brain Aβ accumulation that precedes the onset of clinical symptoms by two decades is considered to trigger the pathogenic cascade for AD development (3). Follow-up studies of discontinued anti-Aβ immunotherapy clinical trials showed that clearance of deposited Aβ plaques was ineffective at either reversing or impeding disease progression, even in the earlier phase of clinical manifestation; these results highlight the need for interventions that prevent brain Aβ accumulation in the preclinical stage (4). However, the preclinical stage (based on biomarker transition) that constitutes the critical period when disease progression should be modified is currently undetermined. This stage must be identified if therapy is to be effective, while a comprehensive list of risk molecules and an understanding of the mechanisms by which these molecules are involved in the pathogenic process are also required.

Integrative analyses of genetic susceptibility loci and differentially expressed genes or pathways have revealed the molecular groups or modules in which expressional changes are associated with AD development (5, 6). These modules include the synaptic transmission, immune response, lipid metabolism, endocytosis, and cell adhesion molecule pathways in addition to amyloid pathology (7). However, this knowledge does not address which changes are primarily involved in AD risk and which

are reactive responses to upstream events. On the other hand, several molecules are reported to be involved in or to influence the metabolism and neurotoxicity of Aβ. Although the intrinsic regulation mechanism for Aβ production in the brain remains to be elucidated, the secretory protein FAM3C is a candidate for an endogenous Aβ suppressor. In previous studies, we found that FAM3C binds to presenilins, catalytic components of the γ-secretase complex, and shows suppressive activity on Aβ production by enhancing nonspecific degradation of the β-secretase-cleaved immediate Aβ precursor without inhibiting secretase activities (8). Moreover, an increase and decrease in FAM3C expression levels in cultured cells led to the down- and upregulation of Aβ secretion, respectively (8). FAM3C is widely expressed in the neuronal cells of the mammalian brain; higher-level distribution of FAM3C protein is typical found in AD lesions such as in the entorhinal cortex and hippocampus (9). Neuronal FAM3C is enriched in presynaptic terminals (9), and the extracellular release of both FAM3C and Aβ is dependent on neuronal activation, specifically on tetanus toxin-sensitive exocytosis of synaptic vesicles in specific synapse subtypes (10).

We previously reported that FAM3C protein expression is downregulated in the autopsied brains of patients with AD compared with the brains of age-matched nondemented or non-AD disease controls (8, 9). In addition, the FAM3C levels of the cerebrospinal fluid were significantly reduced in patients with mild cognitive impairment as well as in those with AD (10). By contrast, the transgenic overexpression of FAM3C ameliorated brain Aβ burden and memory deficits without perturbing Notch

signaling in AD model mice (8). Based on these findings, we hypothesized that the expressional reduction in FAM3C could be a risk factor for brain Aβ accumulation and that the induction of FAM3C expression in the brain might be beneficial to AD cases in the early or preclinical phase. The present study, therefore, aimed to clarify the mechanism underlying the downregulation of FAM3C expression in the AD brain. We revealed that SP1 and EBF1 are involved in the basal expression of FAM3C, and that FAM3C transcription is downregulated in the AD brain through the reduced nuclear levels and genomic DNA-binding abilities of SP1 and EBF1.

Results

FAM3C mRNA levels are decreased in AD brains

Previously, we reported an expressional decline in FAM3C protein in the AD brain relative to control protein levels (8-10). In the present study, to clarify whether this decline was due to transcriptional downregulation, we extracted quantitative data from whole transcriptome sequencing libraries on FAM3C mRNA levels in the frontal cortices of 29 cases with AD and 21 age-matched cognitively healthy subjects. Figure 1 shows that FAM3C mRNA was significantly reduced in AD cases; notably, a marked decline was observed in advanced stages of the Braak neuropathological criteria (11).

Promoter activity in the upstream region of human *FAM3C*

The human *FAM3C* gene, located on chromosome 7q31.31, includes 10 exons that span ~47.5 kb. To identify the *FAM3C* promoter sequence that is sufficient for basal transcriptional activity, we employed a luciferase reporter assay in human nonneuronal HEK293 cells, which endogenously express FAM3C mRNA under physiological conditions. We obtained a bacterial artificial chromosome clone (ID: RP11-369F21; BACPAC Resource Center) that contained the upstream region of the human *FAM3C* gene. The transcription start site (TSS) was retrieved by an *in silico* search in the Database of Transcriptional Start Sites (https://dbtss.hgc.jp). Hereafter, all positions within the 5′-flanking sequence are indexed relative to this +1 TSS. Using the luciferase reporter assay, we identified an 8.8-kb genomic fragment upstream of the TSS that showed promoter activity (Figure 2A, B). This genomic region was divided into approximately 1-kb-long serial fragments, of which the promoter activities were then evaluated under equivalent transfection efficiencies. Three fragments between −4072 and −2940, −2060 and −1002, and −1027 and −1 showed higher luciferase activity (Figure 2B). Subsequently, we narrowed down the candidate promoter sequences from these fragments (Figure 2C–E). Four 5′-flanking regions at −3095 to −3058, −2976 to −2940, −1044 to −1002, and −114 to −1 showed obvious promoter activity.

Delineation of the basal promoter sequence of *FAM3C*

To delineate promoter sequences, we tested internal deletions of the four aforementioned 5′-flanking regions. Among them, the deletion of the −114 to −1 sequence aborted the basal promoter

activity; however, the other deletions did not affect basal activity (Figure 3A). We speculate that a longer genomic distance (>1 kb) from TSS abolished the contribution to basal transcriptional activity. Reporter assays for shorter serial internal deletions in the −163 to −1 fragment further indicated that the sequences from −111 to −101 and from −40 to −20, hereafter referred to as putative promoters A and B, respectively, were required for basal transcriptional activity (Figure 3B). Similar trials for delineation of the basal promoter sequence using human neuronal SH-SY5Y cells and primary mouse neurons produced equivalent results (Supple. Figs. 1 and 2). The deletions of putative promoters A and/or B in HEK293, SH-SY5Y, murine nonneuronal NIH3T3, and murine neuronal Neuro-2a cells led to similar reductions in promoter activity, whereas the deletion of putative promoter A reduced activity to a lesser extent in murine cells than it did in human cells (Figure 3C). Furthermore, substitution of three serial nucleotides in putative promoter B indicated that the −40 to −23 sequence was minimally indispensable for basal transcriptional activity in HEK293 cells (Figure 3D). Substitution of nucleotides −111 to −109 reduced transcriptional activity but did so to a lesser extent (data not shown).

SP1 and EBF1 are candidate transcription factors for *FAM3C*

The nucleotide sequence of the basal promoter is highly conserved between human and mouse genomes (Figure 4A). We searched for transcription factors using DNA-binding profile databases such as cisRED, JASPAR 2018, Genomatix, and TRANSFAC; hits contained SP4, EBF1, ERG1, SMAD1,

KLF6, and SP1 (Figure 4A). Knockdown of SP1 or EBF1 in cultured cells markedly suppressed endogenous expression of FAM3C protein (Figure 4B), whereas overexpression of these transcription factors boosted FAM3C levels (Figure 4C). These results suggested that SP1 and EBF1 drove basal transcription of *FAM3C*. In contrast, KLF6 knockdown upregulated FAM3C expression (Figure 4B). KLF6 reportedly acts as a transcription repressor through recruitment of a corepressor complex containing LCoR (12). Consistent with this, LCoR knockdown also enhanced FAM3C expression (Figure 4D), whereas KLF6 overexpression did not solely induce FAM3C (Figure 4C); however, there was no additive effect when KLF6 and LCoR were simultaneously knocked down (Figure 4D). Knockdown and overexpression of SMAD1 did not significantly affect FAM3C expression, but transfection with the constitutively active mutant of SMAD1 [SMAD1-S463D/S465D (13)] augmented FAM3C expression (Figure 4C). Hence, SMAD1 was considered a candidate inducible transcription factor for *FAM3C*.

SP1 and EBF1 directly bind to the basal promoter sequence

Chromatin immunoprecipitation (ChIP) coupled with quantitative PCR (qPCR) was performed to demonstrate direct binding between candidate basal transcription factors and the basal promoter region of human *FAM3C*. The upstream sequence containing the basal promoter region of SH-SY5Y cells was immunoprecipitated with antibodies against SP1 or EBF1 (Figure 4E). An electrophoretic mobility shift

assay (EMSA) was also performed using total nuclear protein extracts from HEK293 cells and a DNA probe containing the basal promoter sequence (−40 to −23). Formation of a nuclear protein–DNA probe complex was observed as supershifted bands of the biotinylated probe, of which specificity was demonstrated using a competition experiment with a 200-fold molar excess of the unlabeled probe (Figure 4F). To examine whether SP1 and EBF1 were contained in the binding proteins, we performed shift-western blotting. The shifted bands were obviously labeled by antibodies against SP1 and EBF1 (Figure 4G). These results indicated that SP1 and EBF1 were endogenous basal transcription factors of FAM3C.

Genomic deletion of the basal promoter sequence of cultured cells

To assess the basal transcriptional activity of putative promoters A and B directly *in vivo*, their genomic sequences were deleted from HEK293 cells using the CRISPR/Cas9 technique (Figure 5A). The cloned cell lines (H3-4 and H1-135) harboring partial deletions of putative promoter B exhibited approximately 60%–80% reductions in basal expression levels of FAM3C protein, whereas deletion of putative promoter A caused a 10% decrease (Figure 5B). An additive effect of these sequence deletions was observed: the cell line H8-9 harboring the double deletion showed a reduction of ~90% in FAM3C expression (Figure 5B). Knockdown or overexpression of EBF1, SP1, SMAD1, and KLF6 did not alter expression levels of FAM3C protein in the H1-135 cell line (Figure 5C, D). We also generated Neuro-

2a cell lines with deletions of these promoter regions (Supple. Fig. 3A). In each of two selected cell lines, we found six different deletions around putative promoter B; consistently, Neuro-2a cells are known to have unstable karyotypes. Both cell lines exhibited a decrease in endogenous FAM3C levels of >80% (Supple. Fig. 3B). These results indicated that the 5′-flanking sequence between −40 and −23 was the main basal promoter for *FAM3C* and that SP1 and EBF1 are the primary constitutive transcription factors for the gene.

Reduction in the nuclear levels and DNA-binding abilities of SP1 and EBF1 in AD brains

To determine the mechanism underlying transcriptional downregulation of FAM3C in the AD brain, we evaluated the expression levels of SP1, EBF1, and KLF6 in autopsied human brains. RNA-sequencing data (obtained as described in Figure 1) indicated that mRNA levels of EBF1 and KLF6 in AD brains were equivalent to those in control brains, whereas the SP1 mRNA level was slightly increased in AD brains (Figure 6A). Accordingly, we conducted genomic DNA methylation analysis, in which neuronal nuclei isolated from temporal cortex tissues of autopsied brains were assessed (14), and did not find any difference between AD and control samples in terms of methylation patterns around the CpG island of *FAM3C* (Supple. Fig. 4).

In contrast, semiquantitative immunoblotting of nuclear extracts from temporal cortex tissues revealed that SP1 and EBF1 in AD brains were significantly reduced relative to SP1 and EBF1 in the

controls (Figure 6B). We also investigated the DNA-binding abilities of nuclear SP1 and EBF1 extracted from autopsied brains. Shift-western analysis employing a DNA probe containing the basal promoter sequence indicated that the DNA-bound SP1 and EBF1 were significantly diminished in AD cases (Figure 7A, B). In addition, we performed ChIP-qPCR assays using autopsied brain tissues and confirmed the decreased levels of SP1- and EBF1-bound genomic fragments containing the *FAM3C* promoter in AD brains (Figure 7C). Moreover, similar ChIP-qPCR assays indicated that binding between SP1 and the *DHFR* promoter (15) or between EBF1 and the *FBRSL1* promoter (16) was reduced in AD brains compared with the binding detected in control brains (Figure 7D, E). These results revealed that the nuclear levels of SP1 and EBF1 were reduced; moreover, they showed that the unidentified modifications of these proteins perturbed their binding with genomic DNA in AD brains.

Discussion

Our study reveals that FAM3C expression is transcriptionally downregulated in the AD brain. The 5′ upstream sequence (CCGCCAGGGGGCGG/TGCGC) was primarily responsible for the basal transcriptional activity of *FAM3C* in human and mouse, neuronal and nonneuronal, cultured cells. SP1 and EBF1 bind to this basal promoter and sustain endogenous *FAM3C* expression. SMAD1 and KLF6 are the putative inducible transcription factor and transcription repressor for the *FAM3C*, respectively. SP1 and EBF1 in the nuclear extracts from AD brains exhibited reduced protein levels and lower abilities

to bind with the promoter DNA relative to equivalent SP1 and EBF1 from control brains. Transcriptional downregulation in the AD brain is possibly attributable to the insufficient activities of these factors.

FAM3C is ubiquitously expressed at mRNA and protein levels (9, 17). Previous transcriptomic studies have listed *FAM3C* among the downregulated genes found in AD brains [see the supplementary tables in (18, 19)]. However, the regulatory mechanism of FAM3C transcription remains unexamined. The proximal 5′-flanking region of the human *FAM3C* gene lacks a TATA box and contains GC-rich sequences including GGGCGG, which is characteristic of housekeeping genes that are constitutively expressed or involved in growth regulation (17, 20). A recent study reported that transcriptional induction of FAM3C in melanoma cells contributes to invasiveness *in vivo*. HOXB4 (USF-1) directly interacts with the E-box located at 193 to 129 bp upstream of the TSS to induce FAM3C expression and cellular invasive activity (21). However, HOXB4 is expressed at very low levels in mammalian adult brains, especially in the cerebral cortex and hippocampus, which are the main areas of lesions in the AD brain (22).

Our results indicate that SP1 and EBF1 contribute to the basal expression of FMA3C. SP1 is a general transcription factor that can activate or repress transcription in response to physiologic and pathological stimuli. Two previous studies investigated SP1 expression in AD brains using immunoblotting of frontal cortex lysates prepared from autopsied brains; the results were inconsistent, i.e., no change and a 2-fold increase in AD brains relative to control brains, respectively (23, 24). Our

RNA-sequencing results indicated a slight increase in SP1 in the AD brain; however, semiquantitative immunoblotting of nuclear protein extracts revealed that SP1 levels were obviously reduced in AD brains. Superficially, these results are inconsistent; however, it should be noted that, in a previous immunohistochemical study (24), SP1 protein was colocalized with pathological deposits of tau aggregates such as neurofibrillary tangles, dystrophic neurites, and neuropil threads in AD brains. Considering this finding, we speculate that sequestration of SP1 protein by tau aggregates in the cytoplasm or neurites causes a reduction in nuclear SP1 in the AD brain, whereas total SP1 levels remain unchanged or even upregulated.

A previous meta-analysis of gene expression profiling revealed that the pathways enriched by AD-related genes were largely common to those enriched by aging-related genes and that many of these genes were expressed under regulation of SP1 (25). In another study, expression levels of SP1 were also downregulated in senescent cells or aged tissues; levels of promoter-bound SP1 protein were especially reduced in senescent fibroblasts relative to levels in presenescent fibroblasts (26). In addition, studies employing EMSAs revealed that the DNA-binding efficiency of SP1 was reduced in the brains of aged rats relative to in the brains of young rats, which is likely caused by undetermined posttranslational mechanisms but not by decreased *de novo* synthesis of SP1 protein (27, 28). The results of our EMSAs additionally suggest that the efficiency of SP1 was reduced in the AD brain.

EBF family proteins are helix-loop-helix transcription factors and include four members that are critical for lineage specification in early B cell development. When aged mice were compared with young mice, two-fold downregulation of EBF1 expression was found in common lymphoid progenitors of the former relative to the latter (29). Although EBF1 plays an essential role in neural differentiation during the developmental stage, its physiological function in the mature brain has yet to be identified (30, 31). Specific expressional changes in the AD brain have not been described, but the *Caenorhabditis elegans* ortholog (*unc-3*) of EBF1 is known to be downregulated by pan-neuronal overexpression of proaggregating tau and $A\beta_{42}$ peptide (32).

To date, no genetic variants of *FAM3C, SP1,* and *EBF1* have been shown to be associated with AD. However, unidentified genetic variations might indirectly contribute to FAM3C downregulation in the AD brain because the heritability of late-onset sporadic AD has been estimated at 60%–80% according to studies on identical twins (33). Revealing the primary causes of SP1 and EBF1 hypofunction in the AD brain will require further investigation, whereas SMAD1 and KLF6 are unlikely pathophysiologically relevant to the downregulation of FAM3C basal expression in the AD brain. SMAD1 is a candidate inducible transcription activator, whereas the mRNA level of KLF6 repressor was unaltered in AD brains relative to levels in the control.

A previous study revealed that, when activated, TGF-β interferes with the translational silencing of FAM3C and induces the epithelial–mesenchymal transition of mammary epithelial cells

(34). Thus, heterogeneous nuclear ribonucleoprotein E1, which represses FAM3C translation by binding with the 3′ untranslated region of its mRNA, is released from the mRNA by activated TGF-β (34). The SMAD family is known to contain downstream transducers of TGF-β and BMP signaling. The canonical downstream pathway of TGF-β is through SMAD2 and SMAD3, and TGF-β induces the phosphorylation of SMAD1 and SMAD5 only in limited situations, such as epithelial-to-mesenchymal transition (35). Our results indicate the possibility that activated SMAD1 induces *FAM3C* transcription, but so far there is no report showing that activation of TGF-β signaling induces FAM3C expression at the transcriptional level.

This study has some limitations. First, we examined the transcriptional mechanism of *FAM3C* using cultured cells. Additional experiments will be required to confirm that *FAM3C* transcription in mammalian neurons *in vivo* is regulated by the same mechanism as that observed in cultured cells. Moreover, our search for transcription factors using DNA-binding profile databases may have failed to identify all of the transcription factors involving *FAM3C* transcription. However, the simultaneous knockdown of SP1 and EBF1 markedly suppressed the endogenous expression of FAM3C in cultured cells (Figure 4B), suggesting that these are major basal transcription factors. Another constraint of our study was the limited number of autopsied brains analyzed. Furthermore, all participants in the postmortem studies were of Japanese ethnicity. A future investigation with a larger number of brains obtained from a wider spectrum of ethnic groups will be crucial to validate our conclusions.

Prevention or treatment of brain Aβ deposition in the preclinical stage is recognized as essential for the development of disease-modifying AD therapies. According to our previous studies (8-10) and the current work, diminished expression of FAM3C in elderly brains might be a potential risk for Aβ accumulation, whereas interventions to induce FAM3C expression or enhance FAM3C-like activity in the brain may be beneficial to early AD cases.

Materials and Methods

Transcriptome analysis of postmortem brain tissues

Frontal cortex tissues were dissected from the autopsied brains of AD patients (n = 29) and non-demented controls without neurological diseases (n = 21). The subjects were neuropathologically classified according to the neurofibrillary tangle staging of Braak and Braak (11). Total RNA was extracted using the TRIzol Plus RNA Purification System (Thermo Fisher Scientific, Waltham, MA, USA). An Agilent 2100 Bioanalyzer instrument (Agilent Technologies, Santa Clara, CA, USA) was used to obtain the RNA integrity number (RIN). A TruSeq Stranded mRNA Library Prep Kit (Illumina, San Diego, CA, USA) was used for library preparation, which was followed by sequencing on an Illumina NestSeq500. The 75-bp paired-end sequenced reads were aligned to the human transcriptome GRCh38 (release 85 from Ensembl) using *Salmon* (version 0.8.0) as an aligner. Differential expression of genes of interest was analyzed via the *DESeq2* (version 1.14.1) package, with adjustments made for

potential confounding factors: age at death, gender, *APOE* genotypes, and RIN. *P*-values were calculated using the likelihood ratio test and adjusted with the Benjamini-Hochberg procedure for multiple testing correction. The study was approved by the Ethics Committee of Niigata University (2018-0034).

Plasmids and siRNA

The bacterial artificial chromosome clone carrying the human *FAM3C* genomic locus (Clone ID: RP11-369F21) was obtained from BACPAC Resource Center (Children's Hospital Oakland Research Institute, Oakland, CA, USA). The 5′ upstream fragments of *FAM3C* were amplified by PCR and subcloned into the dual-luciferase reporter plasmid pGL4-*Luc2*-TK-*hRluc*, which contained the promoterless firefly luciferase gene of pGL4.10 (Promega, Madison, WI, USA) and TK-promoter-driving *Renilla* luciferase gene of pGL4.74 (Promega) (Figure 1A). Substitutions or deletions were introduced using PCR-based mutagenesis. Human cDNA for SP1, SP4, KLF6, and SMAD1 were amplified by reverse transcription-PCR from total RNA isolated from SH-SY5Y cells. Human cDNA for EBF1 and EGR1 was obtained from RIKEN BioResource Research Center (Tsukuba, Japan). Each cDNA was subcloned into the expression plasmid pCAGEN (36). The constitutively active mutant SMAD1 (SMAD1-S463D/S465D) was generated by PCR-based site-directed mutagenesis (37).

The following siRNA duplexes were purchased from Dharmacon (Lafayette, CO, USA): siGENOME SMART pool M-011848 for human EBF1, M-026959 for human SP1, M-012723 for

human SMAD1, M-021441 for human KLF6, M-040633 for mouse Sp1, M-043282 for mouse Sp4, M-045017 for mouse Ebf1, M-043530 for mouse Klf6, M-040286 for mouse Egr1, M-055762 for mouse Smad1, M-059377 for mouse Lcor, and D-001206 for a nontargeting control.

Luciferase reporter assay

HEK293, SH-SY5Y, Neuro2a, and NIH3T3 cells, or mouse primary cultured neurons on 24-well culture plates were transfected with 50 ng of the indicated reporter plasmid. The cells were harvested after 48 h, and the firefly and *Renilla* luciferase activities in cell lysates were measured using a Dual-Luciferase Reporter Assay system (Promega) on a Nivo microplate reader (PerkinElmer Life Science, Waltham, MA, USA). The resultant data represent firefly luciferase activity normalized by *Renilla* luciferase activity.

Immunoblotting

Immunoblotting was performed as previously described (38). Protein concentrations were measured using a modified Lowry method and the same amounts of total protein were separated by SDS-PAGE. The primary antibodies used were as follows: mouse monoclonal anti-FAM3C (42C1) (10), mouse monoclonal anti-SP1 (Santa Cruz Biotechnology, Dallas, TX, USA), rabbit monoclonal anti-EBF1 (Abcam, Cambridge, MA, USA), mouse monoclonal anti-KLF6 (Abcam), mouse monoclonal

anti-EGR1 (Santa Cruz), mouse monoclonal anti-SMAD1 (Santa Cruz), mouse monoclonal anti-SP4 (Santa Cruz), mouse monoclonal anti-GAPDH (Santa Cruz), and mouse monoclonal anti-TBP (Santa Cruz). Band intensity was measured using an ImageQuant LAS 4000 mini chemiluminescence imager (GE Healthcare, Chicago, IL, USA).

ChIP-qPCR analysis

Quantitative ChIP assays were performed as previously described (39) but with slight modifications. In brief, cultured SH-SY5Y cells were collected in phosphate-buffered saline containing a protease inhibitor cocktail (Roche Diagnostics). Then, 50 mg of frozen temporal cortex tissues from autopsied brains were minced with scissors in phosphate-buffered saline. Cells and minced tissues were cross-linked in 1.0% formaldehyde for 10 min and 1.5% formaldehyde for 20 min, respectively, and then 137.5-mM glycine (final concentration) was added to quench cross-linking. The samples were treated with micrococcal nuclease (New England Biolabs, Ipswich, MA, USA), subjected to sonication, and then incubated with mouse monoclonal anti-SP1 antibody (Santa Cruz), mouse monoclonal anti-EBF1 antibody (Santa Cruz), or normal mouse IgG (Santa Cruz, as a negative control). The immunocomplexes were captured with Protein G Sepharose 4 Fast Flow (GE Healthcare). After overnight incubation with gentle mixing at 4ºC, the protein and DNA complex was decrosslinked at 65ºC before DNA purification. ChIP efficiency was measured by quantitative real-time PCR using KOD

SYBR qPCR Mix (Toyobo) and a LightCycler 480 System II (Roche Diagnostics, Mannheim, Germany). The following primer sets were used: 5′-GTCCTCCACCGCCAGGGGGC-3′ (forward) and 5′-TGGCCAGGAGAAAGCCAGCTC-3′ (reverse) for the *FAM3C* promoter region (from −48 to +61); 5′-TCGCCTGCACAAATGGGGAC-3′ (forward) and 5′-AGAACGCGCGGTCAAGTTT-3′ (reverse) for the *DHFR* promoter region (from +386 to +455); or 5′-TACGCGCTGCATGAATCAAT-3′ (forward) and 5′-CTGGTGGGGTTTTCTGAGC-3′ (reverse) for the *FBRSL1* promoter region (from −965 to +895).

Nuclear protein extraction

Nuclear proteins were extracted as previously described (40). Briefly, cultured cells were suspended in a hypotonic buffer (10-mM HEPES at pH 7.9, 1.5-mM $MgCl_2$, 10-mM KCl, and 0.5-mM DTT) containing a protease inhibitor cocktail (Roche Diagnostics). After incubation for 15 min on ice, the samples were adjusted to 0.05% NP-40 and centrifuged for 30 s at 10,000 *g*. The pellet was resuspended in a hypertonic extraction buffer (20-mM HEPES at pH 7.9, 1.5-mM $MgCl_2$, 420-mM NaCl, 0.2-mM EDTA, 25% glycerol, and 0.5-mM DTT) with agitating for 30 min on ice and then centrifuged for 5 min at 20,000 *g* and 4ºC. The resultant supernatants were used as nuclear extracts.

To prepare nuclear extracts from human brains, we obtained frozen temporal cortex tissues of AD patients (n = 20) and age-matched controls without neurologic disease (n = 10) from the Brain Bank

for Aging Research, Tokyo Metropolitan Institute of Gerontology (Tokyo, Japan). Tissues were homogenized using a motor-driven Teflon/glass homogenizer (5 strokes) in a hypotonic buffer and centrifuged for 20 min at 10,000 *g* and 4ºC. The pellets were resuspended in a hypertonic extraction buffer with agitating for 30 min on ice. After centrifugation for 5 min at 20,000 *g* and 4ºC, the supernatants were obtained as nuclear extracts. The Shiga University of Medical Science Review Board approved the study protocol (28-096).

EMSA and shift-western analysis

EMSA was performed as previously described (41) but with slight modifications. The following biotinylated and unlabeled double-stranded oligonucleotides corresponding to 45 to 15 bp upstream from the TSS of human *FAM3C* gene were used for probes. Sense strands were 5′-ctccaCCGCCAGGGGGCGGGCGCGGCttccc-3′ (wild-type) and 5′-ctccaTTACTAAGAAACGAGTGTAACttccc-3′ (unrelated). To prepare a reaction mixture, 10 fmol of DNA probe was incubated with 5 μg of total nuclear proteins in 10 μL of binding solution (20-mM PIPES at pH 6.8, 50-mM NaCl, 1-mM DTT, 0.25-mg/mL BSA, 100-μM $ZnSO_4$, 0.05% NP-40, 4% Ficoll, and 67.5-μg/mL poly–[dI-dC]) for 30 min on ice. The reaction mixture was then separated by 4% nondenaturing PAGE and transferred to a positively charged nylon membrane. Biotinylated probes were detected with a Light Shift Chemiluminescent EMSA Kit (Thermo Fisher Scientific). For gel mobility

shift-western blotting, proteins in EMSA gels were transferred onto a PVDF membrane as peviously decribed (42), and blots were probed by anti-SP1 (Santa Cruz) or anti-EBF1 (Abcam) antibodies.

Genome editing of culture cells

The putative promoter regions of HEK293 and Neuro-2a cell genomes were deleted by CRISPR-Cas9-mediated site-directed gene editing using a Guide-it sgRNA In Vitro Transcription Kit (Takara Bio, Shiga, Japan), Guide-it Recombinant Cas9 (Takara Bio), and TransIT-X2 transfection reagent (Mirus Bio, Madison, WI, USA). The single guide RNAs were designed using CRISPRdirect (https://crispr.dbcls.jp/) as follows: 5′-AAGCCGCGCCCGCCCCCTGG-3′ for the H1-135 cell line, 5′-CCGCTTGGTCCTCCACCGCC-3′ for the H3-4 cell line, 5′-AGAGCGGAGGGAGGGGTCTG-3′ for the cell lines H6-76 and H8-9, 5′-CGGCTCGGTCCTCCACCGCC-3′ for the N1-13 cell line, and 5′-GCGGAGCCGCGCACGCCCCC-3′ for the N2-77 cell line. The antisense single-stranded donor oligonucleotides were 5′-AATGGGCCCCCGCCGCCGGGAAGCCGCGCCCGCCCCCTGGTGGAGGACCAAGCGGGCGCCCGGGCCGGCCAGAGGGAAGG-3′ for H3-4 cells and 5′-GGGCCGGCCAGAGGGAAGGGCCGGAGAGCGGAGGGAGGGGCGCCCACCGCCCCCGGCCAGGCGCTGCACAATCTGAACTT-3′ for H6-76 and H8-9 cells. Cell populations were cloned by limiting dilution. The H8-9 cell line was cloned by additional genome editing from the H1-135 cell line.

Neuron-specific DNA methylome analysis in autopsied brains

Postmortem frozen tissues of the inferior temporal gyrus from AD patients (n = 30) and age-matched normal controls (n = 30) were homogenized with a motor-driven Teflon/glass homogenizer. Neuronal nuclei were isolated by FACS using an anti-NeuN antibody (Millipore, Darmstadt, Germany). Extracted genomic DNA was bisulfate-converted and subjected to genome-wide DNA methylation analysis using an Infinium HumanMethylation450 BeadChip (Illumina) as previously described (14). The University of Tokyo Review Board approved the study protocol (2183-15).

Statistical analyses

Data are expressed as means ± SEMs. Statistical evaluations were performed using Student's *t*-test for two-group comparisons and one-way ANOVA followed by Tukey's Honest Significant Difference (HSD) test for three (or more)-group comparisons.

Supplementary Materials

Supplementary Material is available at HMG online.

Acknowledgments

This work was supported by AMED under Grant Number JP20dm0107141 (to MNi), JP20dm0107142 (to TS), JP20dm0107143 (to TI), JP20dm0207073 (to TI), JP18dm0107103 (to SM), and Grants-in-Aid for Scientific Research from the Ministry of Education, Culture, Sports, Science, and Technology, Japan (20K16491B to NW, 19H03546 to MNi, and 19K21585 to MNi).

Conflict of Interest Statement

The authors declare no competing financial interests.

References

1 Braak, E., Griffing, K., Arai, K., Bohl, J., Bratzke, H. and Braak, H. (1999) Neuropathology of Alzheimer's disease: what is new since A. Alzheimer? *Eur. Arch. Psychiatry Clin. Neurosci.*, **249 Suppl 3**, 14-22.

2 Holtzman, D.M., Mandelkow, E. and Selkoe, D.J. (2012) Alzheimer disease in 2020. *Cold Spring Harb. Perspect. Med.*, **2**.

3 Selkoe, D.J. and Hardy, J. (2016) The amyloid hypothesis of Alzheimer's disease at 25 years. *EMBO Mol. Med.*, **8**, 595-608.

4 Holmes, C., Boche, D., Wilkinson, D., Yadegarfar, G., Hopkins, V., Bayer, A., Jones, R.W., Bullock, R., Love, S., Neal, J.W. *et al.* (2008) Long-term effects of Aβ42 immunisation in Alzheimer's disease: follow-up of a randomised, placebo-controlled phase I trial. *Lancet*, **372**, 216-223.

5 Bagyinszky, E., Giau, V.V. and An, S.A. (2020) Transcriptomics in Alzheimer's disease: aspects and challenges. *Int. J. Mol. Sci.*, **21**.

6 Pimenova, A.A., Raj, T. and Goate, A.M. (2018) Untangling genetic risk for Alzheimer's disease. *Biol. Psychiatry*, **83**, 300-310.

7 Verheijen, J. and Sleegers, K. (2018) Understanding Alzheimer disease at the interface between genetics and transcriptomics. *Trends Genet.*, **34**, 434-447.

8 Hasegawa, H., Liu, L., Tooyama, I., Murayama, S. and Nishimura, M. (2014) The FAM3 superfamily member ILEI ameliorates Alzheimer's disease-like pathology by destabilizing the penultimate amyloid-β precursor. *Nat. Commun.*, **5**, 3917.

9 Liu, L., Watanabe, N., Akatsu, H. and Nishimura, M. (2016) Neuronal expression of ILEI/FAM3C and its reduction in Alzheimer's disease. *Neuroscience*, **330**, 236-246.

10 Nakano, M., Mitsuishi, Y., Liu, L., Watanabe, N., Hibino, E., Hata, S., Saito, T., Saido, T.C., Murayama, S., Kasuga, K. *et al.* (2021) Extracellular release of ILEI/FAM3C and amyloid-β is associated with the activation of distinct synapse subpopulations. *J. Alzheimers Dis.*, **80**, 159-174.

11 Braak, H. and Braak, E. (1991) Neuropathological stageing of Alzheimer-related changes. *Acta Neuropathol.*, **82**, 239-259.

12 Calderon, M.R., Verway, M., An, B.S., DiFeo, A., Bismar, T.A., Ann, D.K., Martignetti, J.A., Shalom-Barak, T. and White, J.H. (2012) Ligand-dependent corepressor (LCoR) recruitment by Kruppel-like factor 6 (KLF6) regulates expression of the cyclin-dependent kinase inhibitor CDKN1A gene. *J. Biol. Chem.*, **287**, 8662-8674.

13 Nojima, J., Kanomata, K., Takada, Y., Fukuda, T., Kokabu, S., Ohte, S., Takada, T., Tsukui, T., Yamamoto, T.S., Sasanuma, H. *et al.* (2010) Dual roles of smad proteins in the conversion from myoblasts to osteoblastic cells by bone morphogenetic proteins. *J. Biol. Chem.*, **285**, 15577-15586.

14 Mano, T., Nagata, K., Nonaka, T., Tarutani, A., Imamura, T., Hashimoto, T., Bannai, T., Koshi-Mano, K., Tsuchida, T., Ohtomo, R. *et al.* (2017) Neuron-specific methylome analysis reveals epigenetic regulation and tau-related dysfunction of BRCA1 in Alzheimer's disease. *Proc. Natl. Acad. Sci. U. S. A.*, **114**, E9645-E9654.

15 Encarnacao, P.C., Ramirez, V.P., Zhang, C. and Aneskievich, B.J. (2013) Sp sites contribute to basal and inducible expression of the human TNIP1 (TNFα-inducible protein 3-interacting protein 1) promoter. *Biochem. J.*, **452**, 519-529.

16 Guilhamon, P., Eskandarpour, M., Halai, D., Wilson, G.A., Feber, A., Teschendorff, A.E., Gomez, V., Hergovich, A., Tirabosco, R., Fernanda Amary, M. *et al.* (2013) Meta-analysis of IDH-mutant cancers identifies EBF1 as an interaction partner for TET2. *Nat. Commun.*, **4**, 2166.

17 Pilipenko, V.V., Reece, A., Choo, D.I. and Greinwald, J.H., Jr. (2004) Genomic organization and expression analysis of the murine Fam3c gene. *Gene*, **335**, 159-168.

18 Li, X., Long, J., He, T., Belshaw, R. and Scott, J. (2015) Integrated genomic approaches identify major pathways and upstream regulators in late onset Alzheimer's disease. *Sci. Rep.*, **5**, 12393.

19 Mostafavi, S., Gaiteri, C., Sullivan, S.E., White, C.C., Tasaki, S., Xu, J., Taga, M., Klein, H.U., Patrick, E., Komashko, V. *et al.* (2018) A molecular network of the aging human brain provides insights into the pathology and cognitive decline of Alzheimer's disease. *Nat. Neurosci.*, **21**, 811-819.

20 Sehgal, A., Patil, N. and Chao, M. (1988) A constitutive promoter directs expression of the nerve growth factor receptor gene. *Mol. Cell. Biol.*, **8**, 3160-3167.

21 Noguchi, K., Dincman, T.A., Dalton, A.C., Howley, B.V., McCall, B.J., Mohanty, B.K. and Howe, P.H. (2018) Interleukin-like EMT inducer (ILEI) promotes melanoma invasiveness and is transcriptionally up-regulated by upstream stimulatory factor-1 (USF-1). *J. Biol. Chem.*, **293**, 11401-11414.

22 Hutlet, B., Theys, N., Coste, C., Ahn, M.T., Doshishti-Agolli, K., Lizen, B. and Gofflot, F. (2016) Systematic expression analysis of Hox genes at adulthood reveals novel patterns in the central nervous system. *Brain Struct. Funct.*, **221**, 1223-1243.

23 Citron, B.A., Dennis, J.S., Zeitlin, R.S. and Echeverria, V. (2008) Transcription factor Sp1 dysregulation in Alzheimer's disease. *J. Neurosci. Res.*, **86**, 2499-2504.

24 Santpere, G., Nieto, M., Puig, B. and Ferrer, I. (2006) Abnormal Sp1 transcription factor expression in Alzheimer disease and tauopathies. *Neurosci. Lett.*, **397**, 30-34.

25 Meng, G., Zhong, X. and Mei, H. (2016) A systematic investigation into aging related genes in brain and their relationship with Alzheimer's disease. *PLoS One*, **11**, e0150624.

26 Kim, S.Y., Kang, H.T., Han, J.A. and Park, S.C. (2012) The transcription factor Sp1 is responsible for aging-dependent altered nucleocytoplasmic trafficking. *Aging Cell*, **11**, 1102-1109.

27 Ammendola, R., Mesuraca, M., Russo, T. and Cimino, F. (1992) Sp1 DNA binding efficiency is highly reduced in nuclear extracts from aged rat tissues. *J. Biol. Chem.*, **267**, 17944-17948.

28 Helenius, M., Hanninen, M., Lehtinen, S.K. and Salminen, A. (1996) Changes associated with aging and replicative senescence in the regulation of transcription factor nuclear factor-κ B. *Biochem. J.*, **318 (Pt 2)**, 603-608.

29 Lescale, C., Dias, S., Maes, J., Cumano, A., Szabo, P., Charron, D., Weksler, M.E., Dosquet, C., Vieira, P. and Goodhardt, M. (2010) Reduced EBF expression underlies loss of B-cell potential of hematopoietic progenitors with age. *Aging Cell*, **9**, 410-419.

30 Lobo, M.K., Karsten, S.L., Gray, M., Geschwind, D.H. and Yang, X.W. (2006) FACS-array profiling of striatal projection neuron subtypes in juvenile and adult mouse brains. *Nat. Neurosci.*, **9**, 443-452.

31 Garel, S., Marin, F., Mattei, M.G., Vesque, C., Vincent, A. and Charnay, P. (1997) Family of Ebf/Olf-1-related genes potentially involved in neuronal differentiation and regional specification in the central nervous system. *Dev. Dyn.*, **210**, 191-205.

32 Wang, C., Saar, V., Leung, K.L., Chen, L. and Wong, G. (2018) Human amyloid β peptide and tau co-expression impairs behavior and causes specific gene expression changes in *Caenorhabditis elegans*. *Neurobiol. Dis.*, **109**, 88-101.

33 Gatz, M., Reynolds, C.A., Fratiglioni, L., Johansson, B., Mortimer, J.A., Berg, S., Fiske, A. and Pedersen, N.L. (2006) Role of genes and environments for explaining Alzheimer disease. *Arch. Gen. Psychiatry*, **63**, 168-174.

34 Chaudhury, A., Hussey, G.S., Ray, P.S., Jin, G., Fox, P.L. and Howe, P.H. (2010) TGF-β-mediated phosphorylation of hnRNP E1 induces EMT via transcript-selective translational induction of Dab2 and ILEI. *Nat. Cell Biol.*, **12**, 286-293.

35 Ramachandran, A., Vizan, P., Das, D., Chakravarty, P., Vogt, J., Rogers, K.W., Muller, P., Hinck, A.P., Sapkota, G.P. and Hill, C.S. (2018) TGF-β uses a novel mode of receptor activation to phosphorylate SMAD1/5 and induce epithelial-to-mesenchymal transition. *Elife*, **7**, e31756.

36 Matsuda, T. and Cepko, C.L. (2004) Electroporation and RNA interference in the rodent retina *in vivo* and *in vitro*. *Proc. Natl. Acad. Sci. U. S. A.*, **101**, 16-22.

37 Tsukamoto, S., Mizuta, T., Fujimoto, M., Ohte, S., Osawa, K., Miyamoto, A., Yoneyama, K., Murata, E., Machiya, A., Jimi, E. *et al.* (2014) Smad9 is a new type of transcriptional regulator in bone morphogenetic protein signaling. *Sci. Rep.*, **4**, 7596.

38 Nakaya, Y., Yamane, T., Shiraishi, H., Wang, H.Q., Matsubara, E., Sato, T., Dolios, G., Wang, R., De Strooper, B., Shoji, M. *et al.* (2005) Random mutagenesis of presenilin-1 identifies novel mutants exclusively generating long amyloid β-peptides. *J. Biol. Chem.*, **280**, 19070-19077.

39 Imakita, N., Kitabatake, M., Ouji-Sageshima, N., Hara, A., Morita-Takemura, S., Kasahara, K., Matsukawa, A., Wanaka, A., Mikasa, K. and Ito, T. (2019) Abrogated Caveolin-1 expression via histone modification enzyme Setdb2 regulates brain edema in a mouse model of influenza-associated encephalopathy. *Sci. Rep.*, **9**, 284.

40 Nishimura, M., Yu, G., Levesque, G., Zhang, D.M., Ruel, L., Chen, F., Milman, P., Holmes, E., Liang, Y., Kawarai, T. *et al.* (1999) Presenilin mutations associated with Alzheimer disease cause defective intracellular trafficking of β-catenin, a component of the presenilin protein complex. *Nat. Med.*, **5**, 164-169.

41 Sambrook, J. and Russell, D.W. (2006) Gel retardation assays for DNA-binding proteins. *CSH Protoc.*, **2006**.

42 Harbers, M. (2015) Shift-western blotting: separate analysis of protein and DNA from protein-DNA complexes. *Methods Mol. Biol.*, **1312**, 355-373.

Legends to Figures

Figure 1. Relative FAM3C mRNA expression was reduced in autopsied AD brains. **(A)** Whole transcriptome sequencing data were obtained using total RNA extracted from the frontal cortex tissues of AD patients (n = 29) and non-demented controls (n = 21). Relative FAM3C mRNA levels from AD and control brains are shown. Student's *t*-test; ***$p < 0.001$ versus the control. **(B)** Autopsied brains of AD and control cases were staged into Braak 0, I–II, III–IV, and V–VI according to the neuropathological criteria (11). FAM3C mRNA levels of Braak stage groups are shown. Boxes, horizontal lines, and whiskers represent interquartile ranges, medians, and maximum/minimum values, respectively.

Figure 2. Luciferase reporter assays for the basal promoter of *FAM3C*. **(A)** Schematic diagram of the pGL4-*Luc2*-TK-*hRluc* plasmid. TSS: transcription start site; Luc2: firefly luciferase gene; hRluc: *Renilla* luciferase gene; p(A): SV40 late polyadenylation signal; TK: HSV-TK promoter; and Stop: stop codon. **(B–E)** Relative luciferase activity of consecutive ~1 kb-long regions in the 5′-flanking sequence **(B)** and truncated sequences of the fragments between −4072 and −2940 **(C)**, between −2060 and −1002 **(D)**, and between −1027 and −1 **(E)**. Each reporter plasmid (50 ng) was transfected into HEK293 cells. The relative activity is shown (n = 3, mean + SEM). One-way ANOVA followed by Tukey's HSD; ***$p <$ 0.001 versus no promoter.

Figure 3. Delineation of the basal promoter sequence of *FAM3C*. **(A–D)** Relative luciferase activity of the 5′-flanking sequence between −4072 and −1 with four different internal deletions **(A)**; the sequence between −631 and −1 with consecutive ~10-bp deletions **(B)**; the sequence between −631 and −1 with deletions of putative promoter A (ΔA), putative promoter B (ΔB), or both (ΔA and ΔB) in indicated cells

(C); and consecutive three-nucleotides substitutions (C to T and G to A) of putative promoter A **(D)**. Relative activity is shown (n = 3, mean + SEM). One-way ANOVA followed by Tukey's HSD; $^{**}p < 0.01$, $^{***}p < 0.001$ versus −4072 to −1 **(A)**, −631 to −1 **(B, C)**, or wild-type (WT) **(D)**.

Figure 4. Evaluation of candidate transcription factors for *FAM3C*. **(A)** The 5′-flanking sequences around the basal promoter of human and mouse *FAM3C* genes. Aligned recognition motifs of candidate transcription factors are shown. **(B–D)** Immunoblots of Neuro-2a cells transfected with siRNAs or expression plasmids for indicated candidates were probed with antibodies against FAM3C or GAPDH. Bar graphs show the relative intensity of FAM3C bands, which are normalized by those of GAPDH (n = 3, mean + SEM). KD, knockdown; OE, overexpression. One-way ANOVA followed by Tukey's HSD; $^{**}p < 0.01$ and $^{***}p < 0.001$ versus the controls (nontargeting siRNA or mCherry plasmid). **(E)** ChIP assays of SH-SY5Y cells with antibodies against SP1 or EBF1 and normal IgG, followed by qPCR with primers targeting the upstream region containing the *FAM3C* promoter sequence. Bar graph shows relative enrichment normalized to input (mean + SEM). Student's *t*-test; $^{***}p < 0.001$ versus normal IgG. **(F)** EMSA using nuclear extract (NE) from SH-SY5Y cells and the biotinylated DNA probe containing the sequence at −40 to −20 of the human *FAM3C* gene. BP: biotinylated probe; UP: unlabeled probe (a 200-fold molar excess). Arrow indicates the shifted band. **(G)** Shift-western analysis using NE from native HEK293 cells (for SP1) and HEK293 cells transfected with EBF1 (for EBF1) and the DNA probe containing the basal promoter sequence and unrelated sequence (U). The arrows indicate the shifted bands. The results are representative of three independent experiments **(B–G)**.

Figure 5. Disruption of the candidate promoter sequences suppressed basal expression of FAM3C and abolished SP1- and EBF1-mediated induction of FAM3C. **(A)** The putative promoter regions of the HEK293 cell genome were disrupted by CRISPR-Cas9-mediated site-directed gene editing. DNA

sequencing of seven independent genomic fragments from each cloned cell line revealed the two deleted alleles shown. WT, wild-type. **(B)** Immunoblots for FAM3C using lysates of cell lines shown in (A). Bar graph shows the relative intensities of FAM3C bands, which are normalized by those of GAPDH (n = 3, mean + SEM). One-way ANOVA followed by Tukey's HSD; $^{**}p < 0.01$ and $^{***}p < 0.001$ versus HEK293. Immunoblots for FAM3C using H1-135 cells transfected with siRNAs **(C)** or expression plasmids **(D)** for indicated transcription factors. Immunoblots for GAPDH served as loading controls. Results are representative of three independent experiments. KD, knockdown; OE, overexpression.

Figure 6. Expression of the candidate transcription factors in AD autopsied brains. **(A)** RNA-sequencing data were obtained as described in Figure 1. Relative mRNA levels of SP1, EBF1, and KLF6 in AD and control brains are shown. Boxes, horizontal lines, and whiskers represent interquartile ranges, medians, and maximum/minimum values, respectively. Student's *t*-test; not significant (ns) and $^{**}p < 0.01$ versus the control (Cont). **(B)** Immunoblots for nuclear SP1, EBF1, and TBP. The same amount of nuclear protein extracted from the frontal cortex homogenates of autopsied brains was subjected to immunoblotting. Bar graph shows the relative intensities of SP1 and EBF1 bands, which are normalized by that of TBP. Student's *t*-test; $^{**}p < 0.01$ versus the control.

Figure 7. The reduced DNA-binding ability of SP1 and EBF1 prepared fin AD brain. For shift-western analysis, the DNA probe containing the basal promoter sequence was incubated with the same amount of total nuclear proteins extracted from frontal cortex homogenates of autopsied brains. The reaction mixture was separated by nondenaturing PAGE and the blots were probed with antibodies against SP1 **(A)** or EBF1 **(B)**. Results are representative of three independent experiments. Bar graphs show the relative intensity of SP1 or EBF1 bands, which are normalized by that of control case #1 in the far left lane of each blot (mean + SEM). Student's *t*-test; $^{*}p < 0.05$ and $^{**}p < 0.01$ versus the control. **(C–E)**

ChIP assays of frozen temporal cortex tissues of autopsied brains with antibodies against SP1 or EBF1 and normal IgG (negative control), followed by qPCR with primer pairs specific to the promoter region of *FAM3C* (C), *DHFR* (D), or *FBRSL1* (E). The same sample set was used as in (A) and (B). Bar graph shows relative enrichment normalized to input (mean + SEM). Student's *t*-test; $*p < 0.05$ and $**p < 0.01$ versus each control.

Abbreviations

AD, Alzheimer's disease;

MCI, mild cognitive impairment;

FAM3C, family with sequence similarity 3, member C;

ILEI, interleukin-like epithelial-mesenchymal transition inducer;

TSS, transcription start site;

EMSA, electrophoretic mobility shift assay;

ChIP, chromatin immunoprecipitation;

qPCR, quantitative polymerase chain reaction;

Figure 1

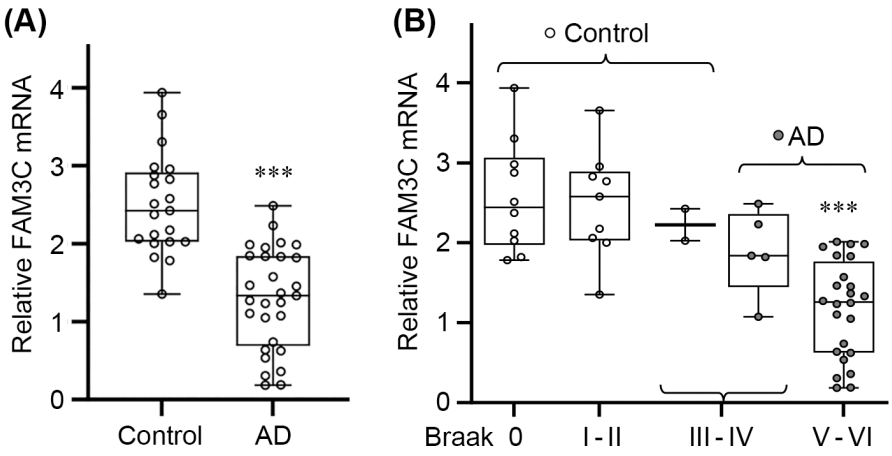
(A)
Relative FAM3C mRNA
0
1
2
3
4
***
Control
AD
(B)
Control
AD
Relative FAM3C mRNA
0
1
2
3
4
***
Braak 0
I - II
III - IV
V - VI

Figure 2

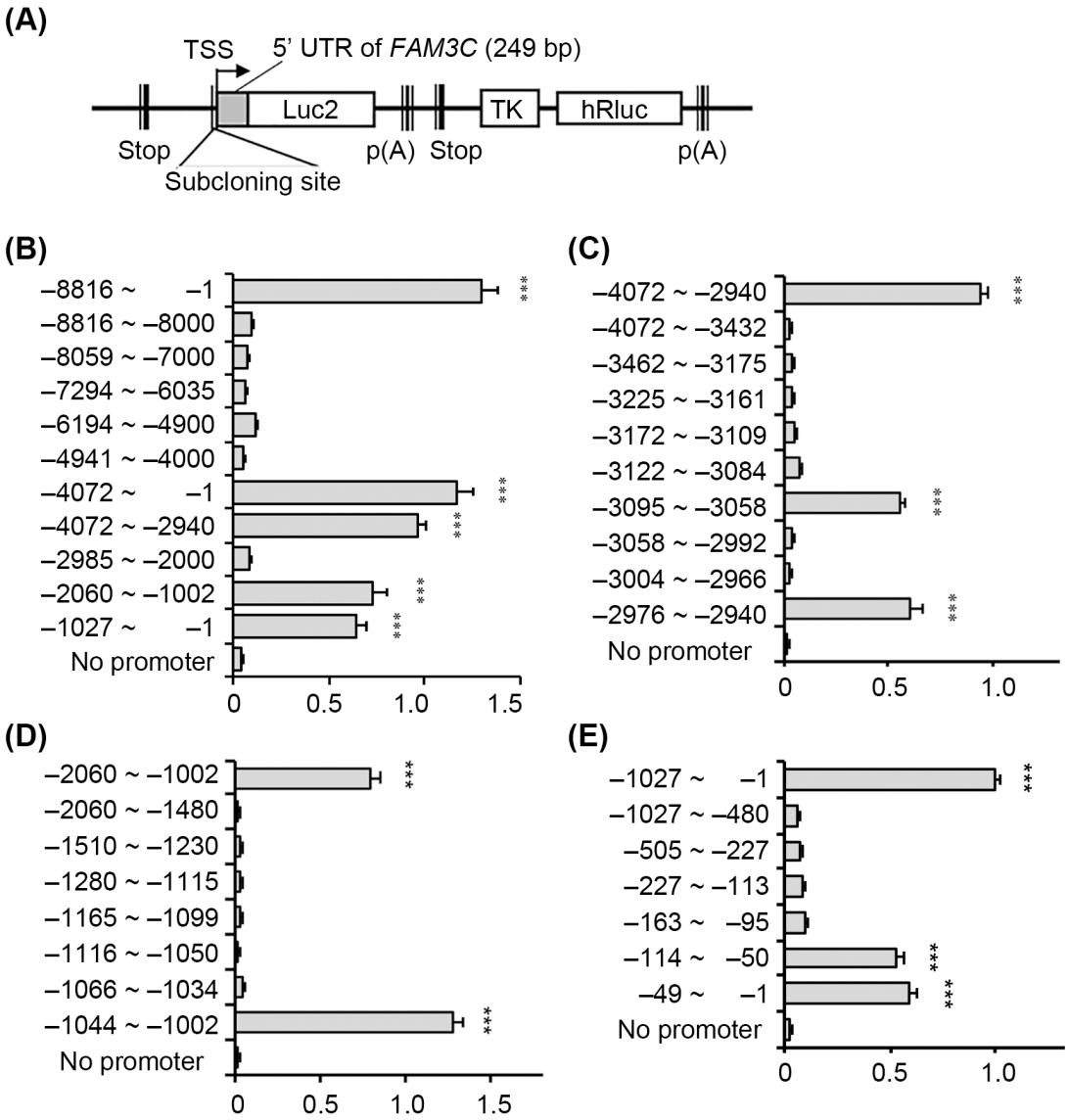
(A)
TSS
5' UTR of FAM3C (249 bp)
Luc2
TK
hRluc
Stop
p(A)
Stop
p(A)
Subcloning site
(B)
–8816 ~ –1
–8816 ~ –8000
–8059 ~ –7000
–7294 ~ –6035
–6194 ~ –4900
–4941 ~ –4000
–4072 ~ –1
–4072 ~ –2940
–2985 ~ –2000
–2060 ~ –1002
–1027 ~ –1
No promoter
0
0.5
1.0
1.5
(C)
–4072 ~ –2940
–4072 ~ –3432
–3462 ~ –3175
–3225 ~ –3161
–3172 ~ –3109
–3122 ~ –3084
–3095 ~ –3058
–3058 ~ –2992
–3004 ~ –2966
–2976 ~ –2940
No promoter
0
0.5
1.0
(D)
–2060 ~ –1002
–2060 ~ –1480
–1510 ~ –1230
–1280 ~ –1115
–1165 ~ –1099
–1116 ~ –1050
–1066 ~ –1034
–1044 ~ –1002
No promoter
0
0.5
1.0
1.5
(E)
–1027 ~ –1
–1027 ~ –480
–505 ~ –227
–227 ~ –113
–163 ~ –95
–114 ~ –50
–49 ~ –1
No promoter
0
0.5
1.0

Figure 3

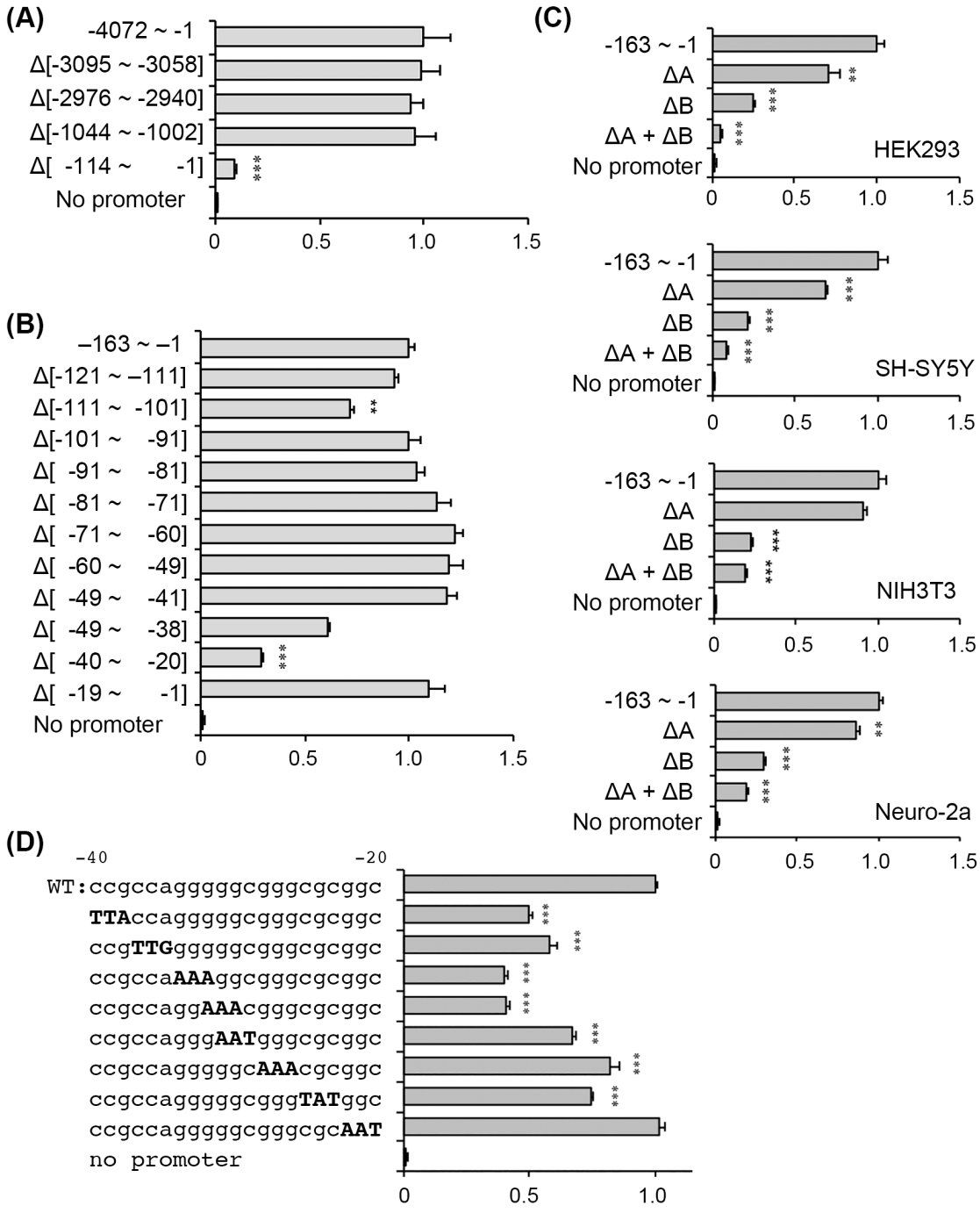
(A)
-4072 ~ -1
Δ[-3095 ~ -3058]
Δ[-2976 ~ -2940]
Δ[-1044 ~ -1002]
Δ[-114 ~ -1]
No promoter
0
0.5
1.0
1.5
(B)
–163 ~ –1
Δ[-121 ~ –111]
Δ[-111 ~ -101]
Δ[-101 ~ -91]
Δ[-91 ~ -81]
Δ[-81 ~ -71]
Δ[-71 ~ -60]
Δ[-60 ~ -49]
Δ[-49 ~ -41]
Δ[-49 ~ -38]
Δ[-40 ~ -20]
Δ[-19 ~ -1]
No promoter
(C)
-163 ~ -1
ΔA
ΔB
ΔA + ΔB
No promoter
HEK293
SH-SY5Y
NIH3T3
Neuro-2a
(D)
-40
-20
WT:ccgccaggggcgggcgcggc
TTAccaggggcgggcgcggc
ccgTTGgggggcgggcgcggc
ccgccaAAAggcgggcgcggc
ccgccaggAAAcgggcgcggc
ccgccagggAATgggcgcggc
ccgccaggggcAAAcgcggc
ccgccaggggcgggTATggc
ccgccaggggcgggcgcAAT
no promoter

Figure 4

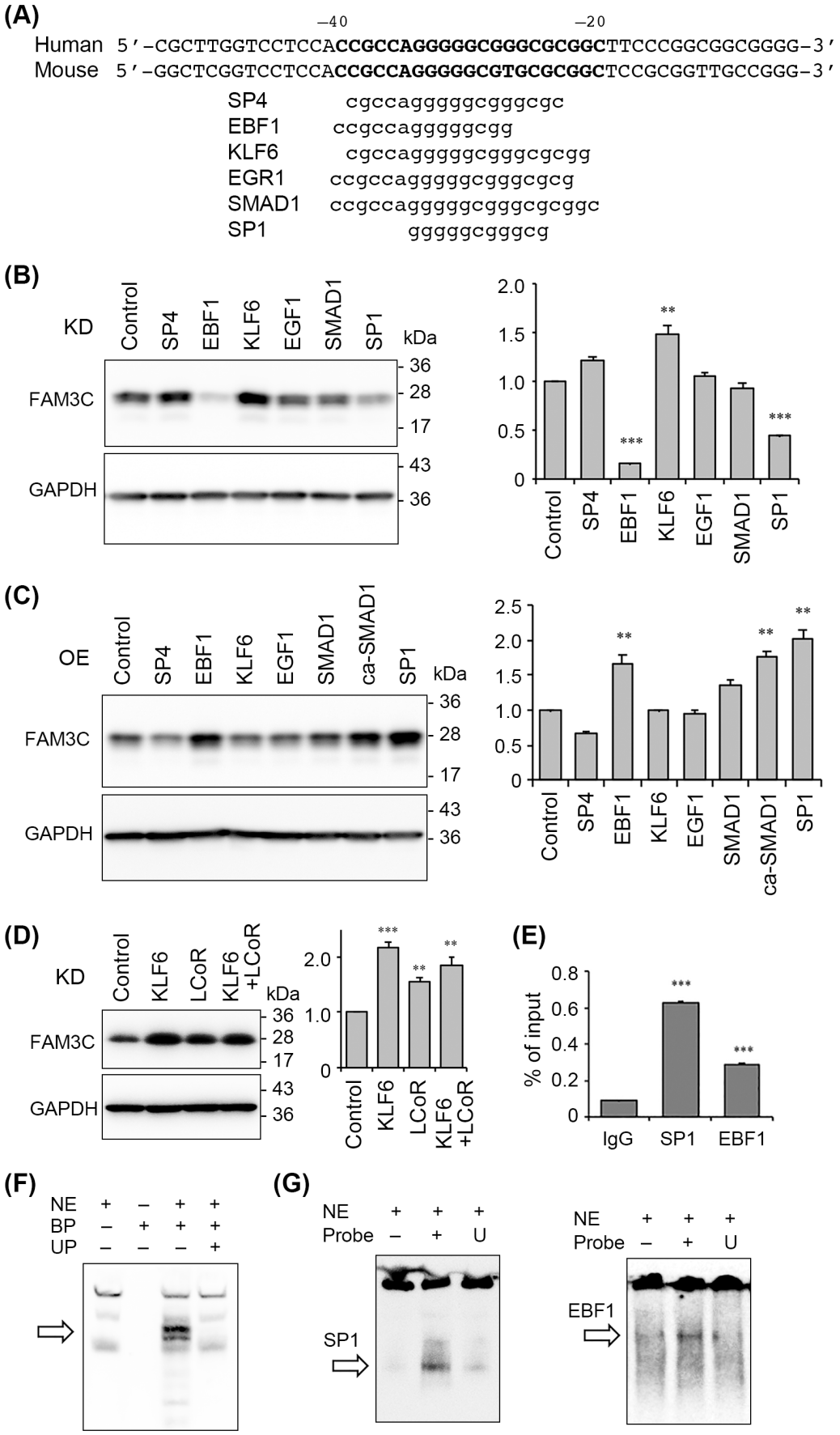
(A)
−40
−20
Human 5′-CGCTTGGTCCTCCACCGCCAGGGGGCGGGCGCGGCTTCCCGGCGGCGGGG-3′
Mouse 5′-GGCTCGGTCCTCCACCGCCAGGGGGCGTGCGCGGCTCCGCGGTTGCCGGG-3′
SP4 cgccaggggcgggcgc
EBF1 ccgccaggggcgg
KLF6 cgccaggggcgggcgcgg
EGR1 ccgccaggggcgggcgcg
SMAD1 ccgccaggggcgggcgcggc
SP1 ggggcgggcg
(B)
KD
Control
SP4
EBF1
KLF6
EGF1
SMAD1
SP1
kDa
FAM3C
GAPDH
36
28
17
43
36
2.0
1.5
1.0
0.5
0
**
***
(C)
OE
ca-SMAD1
2.5
2.0
(D)
KLF6
LCoR
KLF6 +LCoR
(E)
% of input
0.8
0.6
0.4
0.2
IgG
SP1
EBF1
(F)
NE
BP
UP
(G)
Probe
U
EBF1

Figure 5

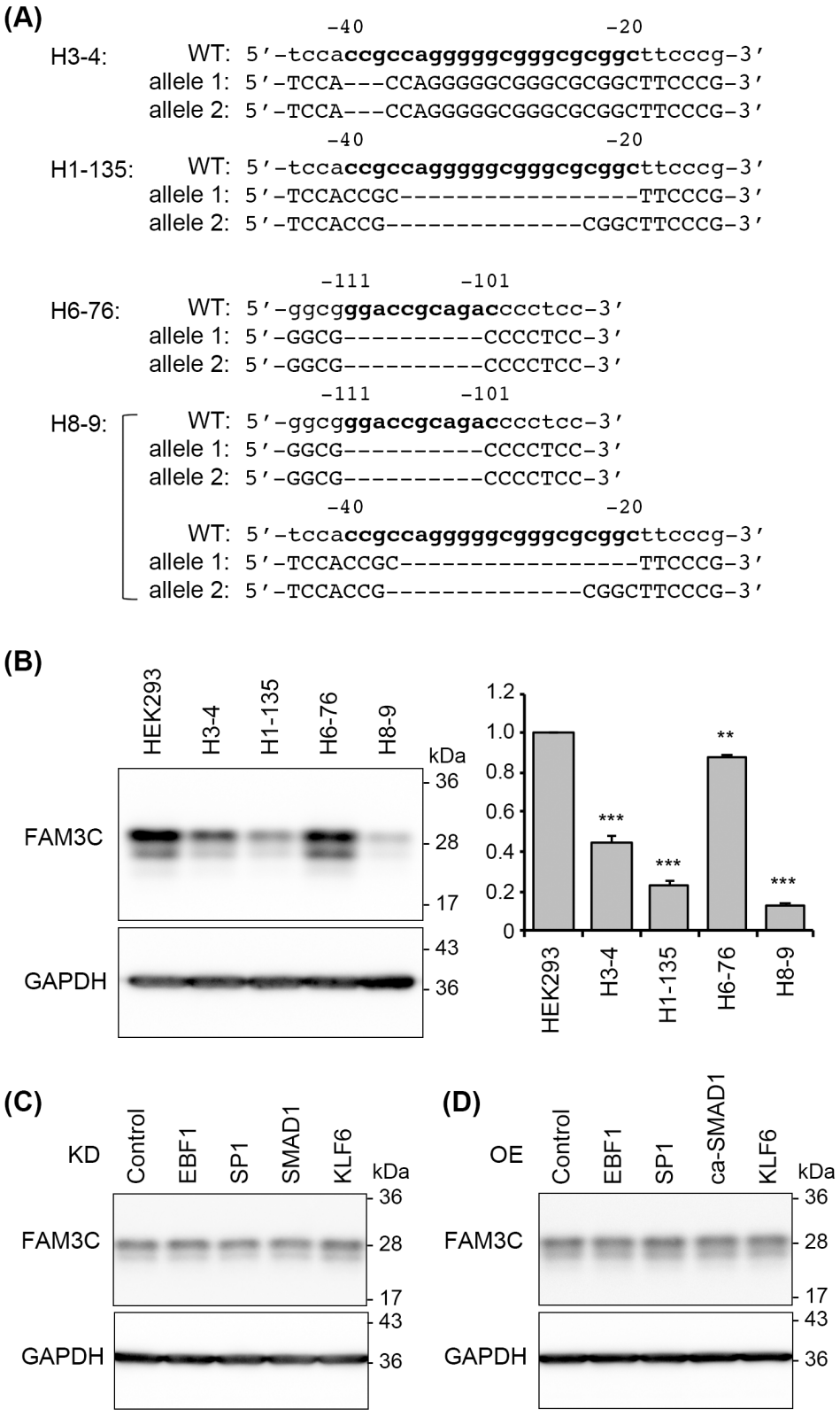
(A)
H3-4:
WT: 5′-tccaccgccaggggcgggcgcggcttcccg-3′
allele 1: 5′-TCCA---CCAGGGGGCGGGCGCGGCTTCCCG-3′
allele 2: 5′-TCCA---CCAGGGGGCGGGCGCGGCTTCCCG-3′
H1-135:
WT: 5′-tccaccgccaggggcgggcgcggcttcccg-3′
allele 1: 5′-TCCACCGC----------TTCCCG-3′
allele 2: 5′-TCCACCG----------CGGCTTCCCG-3′
H6-76:
WT: 5′-ggcggaccgcagaccctcc-3′
allele 1: 5′-GGCG----------CCCCTCC-3′
allele 2: 5′-GGCG----------CCCCTCC-3′
H8-9:
WT: 5′-ggcggaccgcagaccctcc-3′
allele 1: 5′-GGCG----------CCCCTCC-3′
allele 2: 5′-GGCG----------CCCCTCC-3′
WT: 5′-tccaccgccaggggcgggcgcggcttcccg-3′
allele 1: 5′-TCCACCGC----------TTCCCG-3′
allele 2: 5′-TCCACCG----------CGGCTTCCCG-3′
(B)
HEK293
H3-4
H1-135
H6-76
H8-9
kDa
FAM3C
GAPDH
36
28
17
43
36
1.2
1.0
0.8
0.6
0.4
0.2
0
**
***
***
***
(C)
KD
Control
EBF1
SP1
SMAD1
KLF6
kDa
FAM3C
GAPDH
36
28
17
43
36
(D)
OE
Control
EBF1
SP1
ca-SMAD1
KLF6
kDa
FAM3C
GAPDH
36
28
17
43
36

Figure 6

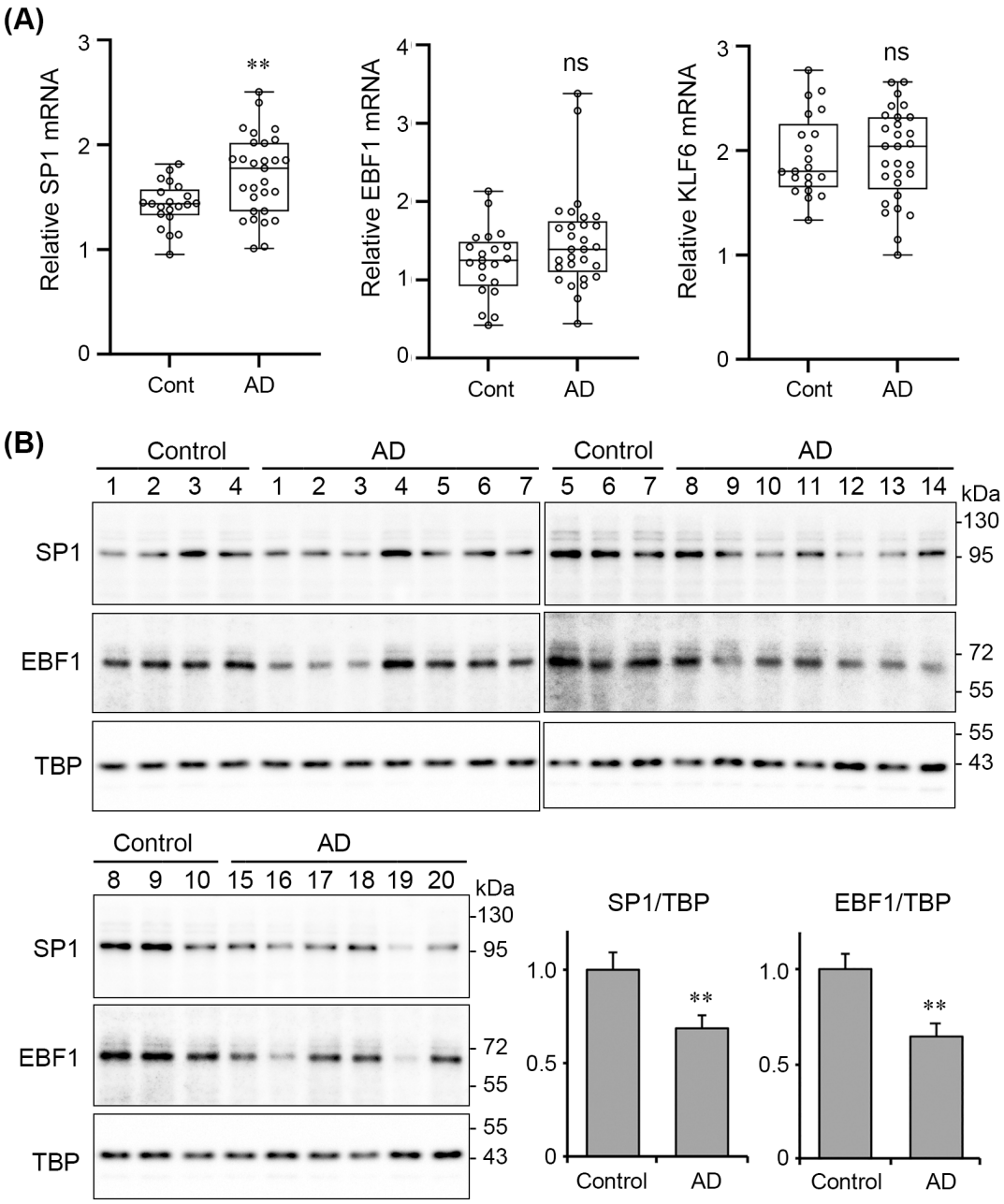
(A)
Relative SP1 mRNA
Relative EBF1 mRNA
Relative KLF6 mRNA
**
ns
ns
Cont
AD
(B)
Control
AD
kDa
SP1
EBF1
TBP
130
95
72
55
43
SP1/TBP
EBF1/TBP
1.0
0.5
0

Figure 7

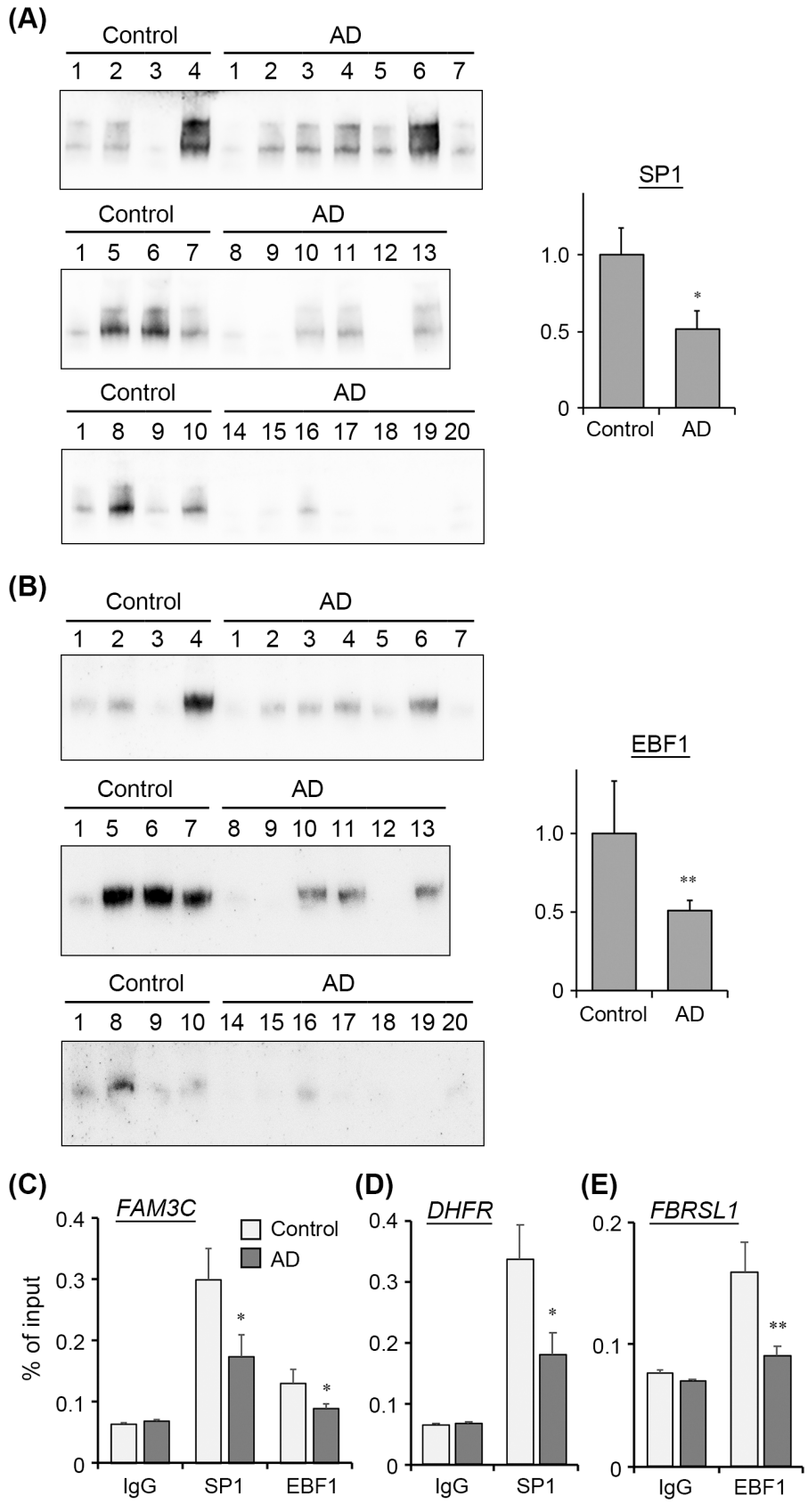
(A)
Control
AD
1 2 3 4 1 2 3 4 5 6 7
Control
AD
1 5 6 7 8 9 10 11 12 13
Control
AD
1 8 9 10 14 15 16 17 18 19 20
SP1
1.0
0.5
0
*
Control
AD
(B)
Control
AD
1 2 3 4 1 2 3 4 5 6 7
Control
AD
1 5 6 7 8 9 10 11 12 13
Control
AD
1 8 9 10 14 15 16 17 18 19 20
EBF1
1.0
0.5
0
**
Control
AD
(C)
FAM3C
Control
AD
% of input
0.4
0.3
0.2
0.1
0
*
*
IgG
SP1
EBF1
(D)
DHFR
0.4
0.3
0.2
0.1
0
*
IgG
SP1
(E)
FBRSL1
0.2
0.1
0
**
IgG
EBF1

Supplementary Figure 1

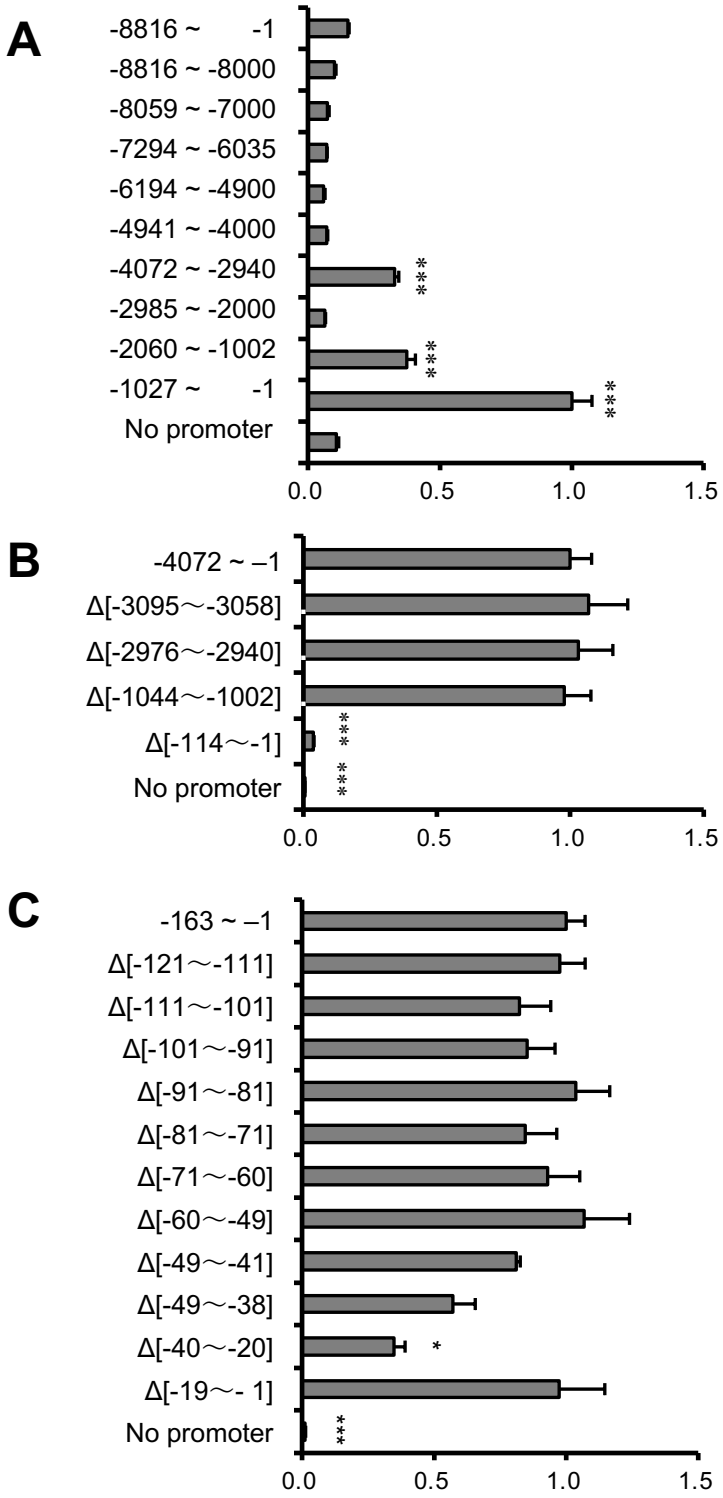

Supplementary Fig. 1

Luciferase reporter assays in SH-SY5Y cells.
Relative luciferase activity of consecutive ~1 kb-long regions in the 5′-flanking sequence **(A)**, the fragment between −4072 and −1 with four different internal deletions **(B)**, and the sequence between −631 and −1 with consecutive ~10-bp deletions **(C)**. Each reporter plasmid (50 ng) was transfected into SH-SY5Y cells. The relative activity is shown (n = 3, mean + SEM). One-way ANOVA followed by Tukey's HSD; ***$p < 0.001$ versus no promoter **(A)** or −4072 to −1 **(B),** *$p < 0.05$, and ***$p < 0.001$ versus −631 to −1 **(C)**.

Supplementary Figure 2

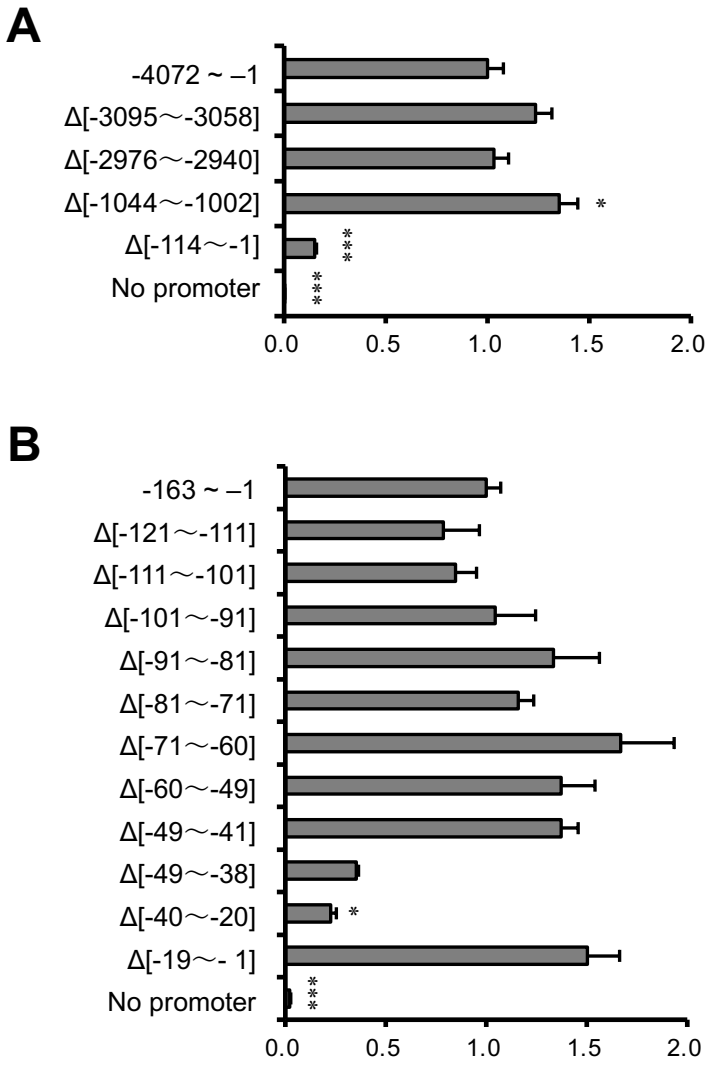

Supplementary Fig. 2

Luciferase reporter assays in primary culture mouse neurons.
Relative luciferase activity of the fragment between −4072 and −14 with four different internal deletions **(A)**, and the sequence between −631 and −1 with consecutive ~10-bp deletions **(B)**. Each reporter plasmid (50 ng) was transfected into neurons. The relative activity is shown (n = 3, mean + SEM). One-way ANOVA followed by Tukey's HSD; *$p < 0.05$, ***$p < 0.001$ versus −4072 to −1 **(A)** or −631 to −1 **(B)**. For preparation of primary cultured neurons, hippocampus and cerebral cortex tissues were dissected from E15.5 C57BL/6J mice. Cells were dissociated with papain (25 units/mL), and then cultured in Neurobasal medium (Gibco, Thermo Fisher Scientific, Waltham, MA, USA) supplemented with GlutaMAX (Gibco), B-27 supplement (Gibco), horse serum (Gibco) and Penicillin/Streptomycin. The mitotic inhibitor cytosine arabinoside (5 μM) was added into the medium after 3 days of culture.

Supplementary Figure 3

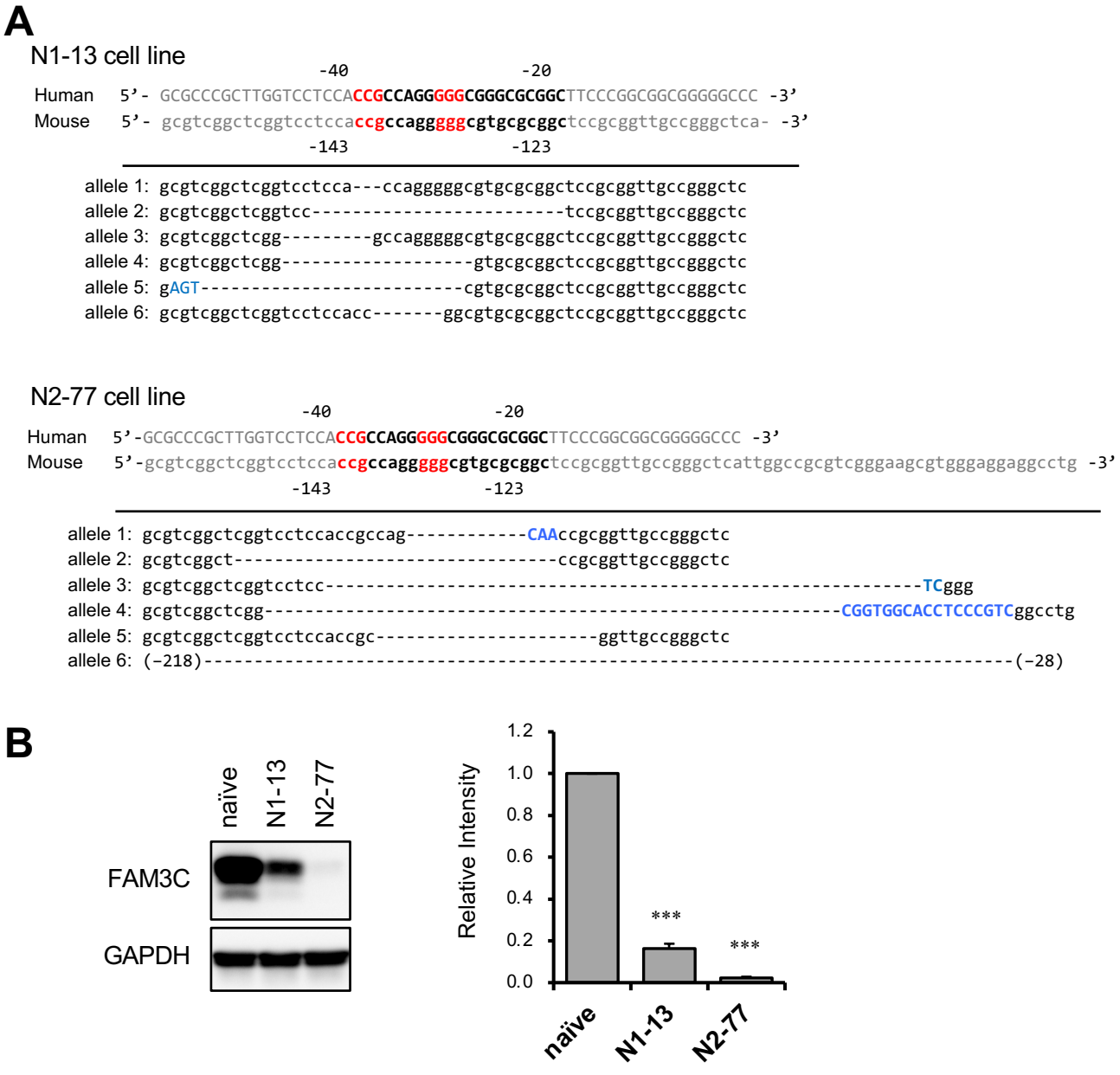

Supplementary Fig. 3

Basal *FAM3C* promoter-disrupted Neuro-2a cell lines

(A) The putative promoter regions of the Neuro-2a cell genome were disrupted by CRISPR-Cas9-mediated site-directed gene editing. DNA sequencing of 19 and 31 independent genomic fragments from N1-13 and N2-77 line lines, respectively, revealed six different deleted alleles shown. The blue capital letters indicate the inserted sequences. **(B)** Immunoblots for FAM3C and GAPDH using N1-13 and N2-77 cell lines. Bar graph shows the relative intensities of FAM3C bands, which are normalized by those of GAPDH (n = 3, mean + SEM). One-way ANOVA followed by Tukey's HSD; ***$p < 0.001$ versus naïve Neuro-2a cells.

Supplementary Figure 4

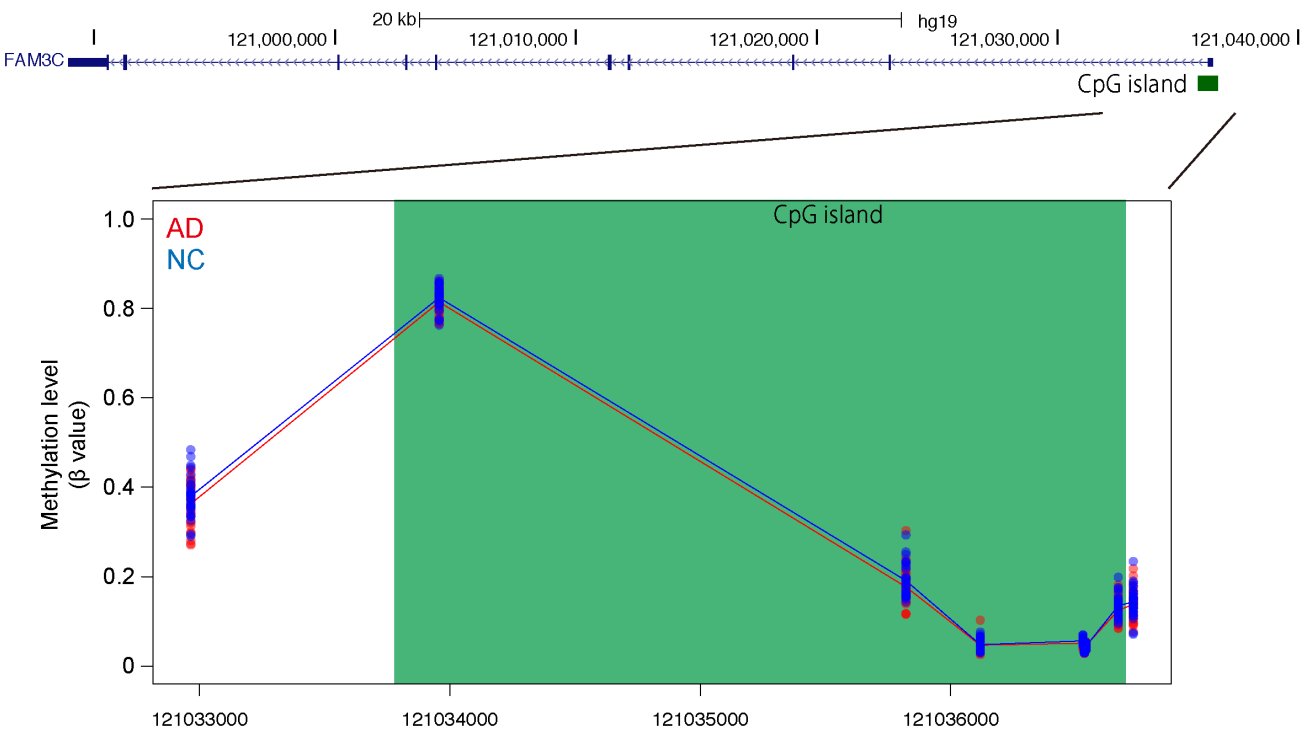

Supplementary Fig. 4

Neuron-specific DNA methylome analysis of the *FAM3C* gene in AD brain
Methylation levels in genomic DNA near the *FAM3C* gene. Genomic DNA was extracted from neuronal nuclei which were prepared from autopsied brains of AD patients (AD; n = 30) and age-matched controls (NC; n = 30). The upper panel shows RefSeq gene map and CpG islands (green bars). The lower panel depicts β values of each sample at the CpG site. Dots are β values from each sample, and solid lines are mean β values of each group. Green area corresponds to the CpG island.